PHYSICAL REVIEW B **105**, L100404 (2022)

Letter

Emergent interlayer magnetic order via strain-induced orthorhombic distortion in the 5*d* Mott insulator Sr_2IrO_4

S. Shrestha,[1] M. Krautloher,[2] M. Zhu,[3] J. Kim,[1] J. Hwang,[3] J. Kim,[4] J.-W. Kim,[4] B. Keimer,[2] and A. Seo[1,*]

[1]*Department of Physics and Astronomy, University of Kentucky, Lexington, Kentucky 40506, USA*
[2]*Max-Planck-Institut für Festkörperforschung, D-70569 Stuttgart, Germany*
[3]*Department of Materials Science and Engineering, The Ohio State University, Columbus, Ohio 43210, USA*
[4]*Advanced Photon Source, Argonne National Laboratory, Argonne, Illinois 60439, USA*

(Received 13 September 2021; accepted 22 February 2022; published 9 March 2022)

We report a La_2CuO_4-like interlayer antiferromagnetic order in Sr_2IrO_4 films with large orthorhombic distortion ($>1.5\%$). The biaxial lattice strain in epitaxial heterostructures of $Sr_2IrO_4/Ca_3Ru_2O_7$ lowers the crystal symmetry of Sr_2IrO_4 from tetragonal (C_4) to orthorhombic (C_2), guiding the Ir 5*d* $J_{\mathrm{eff}} = 1/2$ pseudospin moment parallel to the elongated *b* axis via magnetic anisotropy. From resonant x-ray scattering experiments, we observed an antiferromagnetic order in the orthorhombic Sr_2IrO_4 film whose interlayer stacking pattern is inverted from that of the tetragonal Sr_2IrO_4 crystal. This interlayer stacking is similar to that of the orthorhombic La_2CuO_4, implying that the asymmetric interlayer exchange interactions between *a* and *b* directions exceed the anisotropic interlayer pseudodipolar interaction. Our result suggests that strain-induced distortion can provide a delicate knob for tuning the long-range magnetic order in quasi-two-dimensional systems by evoking the competition between the interlayer exchange coupling and the pseudodipolar interaction.

DOI: 10.1103/PhysRevB.105.L100404

Transition-metal oxides are a featured condensed-matter system for realizing emergent electronic and magnetic phases due to competing interactions and strong electron correlation. Layered oxides with the quasi-two-dimensional K_2NiF_4-type structure are of particular interest since they include superconducting high-T_c cuprates [1,2], spin/charge/orbital ordered manganates [3], spin-orbit coupled iridates [4,5], and so forth. Despite their diverse physical properties, the spin Hamiltonian of the system is commonly described by

$$H_{\mathrm{ij}} = J_{\mathrm{ij}}\,\mathbf{S}_{\mathrm{i}} \cdot \mathbf{S}_{\mathrm{j}} + \mathbf{D}_{\mathrm{ij}} \cdot \mathbf{S}_{\mathrm{i}} \times \mathbf{S}_{\mathrm{j}} + \mathbf{S}_{\mathrm{i}} \cdot \Gamma_{\mathrm{ij}} \cdot \mathbf{S}_{\mathrm{j}}, \tag{1}$$

where the first term is the Heisenberg exchange interaction, the second term is the antisymmetric Dzyaloshinskii-Moriya (DM) interaction, and the third term is the pseudodipolar interaction with symmetric traceless second rank tensor Γ_{ij}, respectively, between two sites *i* and *j* [6]. Because of the quasi-two-dimensional nature of the layered oxides, in-plane interactions are often considered important in theoretical models [7]. This approximation is justified because the Heisenberg exchange interaction within the basal plane is a few orders of magnitude stronger than any interlayer interactions. Nevertheless, it is noteworthy that many layered oxides exhibit long-range magnetic order with well-defined Néel temperature (T_N), which is not allowed in an ideal 2D Heisenberg spin system with continuous symmetry [8]. The interlayer long-range magnetic order is determined by interlayer Hamiltonian, defined as

$$\begin{aligned} H_{\langle i,\,j\rangle//a} &= J^a_{\mathrm{out}}(\mathbf{S}_{\mathrm{i}} \cdot \mathbf{S}_{\mathrm{j}}) + \Gamma^a_{\mathrm{out}}\left(S^a_{\mathrm{i}} S^a_{\mathrm{j}} - S^b_{\mathrm{i}} S^b_{\mathrm{j}}\right) \\ H_{\langle i,\,j\rangle//b} &= J^b_{\mathrm{out}}(\mathbf{S}_{\mathrm{i}} \cdot \mathbf{S}_{\mathrm{j}}) + \Gamma^b_{\mathrm{out}}\left(S^b_{\mathrm{i}} S^b_{\mathrm{j}} - S^a_{\mathrm{i}} S^a_{\mathrm{j}}\right), \end{aligned} \tag{2}$$

where J^a_{out} and J^b_{out} are the nearest interlayer exchange interactions and Γ^a_{out} and Γ^b_{out} are the anisotropic interlayer pseudodipolar interactions along the crystallographic *a* and *b* directions, respectively, as shown in Fig. 1(a). We define j_c and δ_c as the energies from the nearest interlayer exchange interaction and the anisotropic interlayer pseudodipolar interaction, respectively:

$$\begin{aligned} j_c &\equiv J^a_{\mathrm{out}}(\mathbf{S}_{\mathrm{i}} \cdot \mathbf{S}_{\mathrm{j}}) + J^b_{\mathrm{out}}(\mathbf{S}_{\mathrm{i}} \cdot \mathbf{S}_{\mathrm{j}}), \\ \delta_c &\equiv \Gamma^a_{\mathrm{out}}\left(S^a_{\mathrm{i}} S^a_{\mathrm{j}} - S^b_{\mathrm{i}} S^b_{\mathrm{j}}\right) + \Gamma^b_{\mathrm{out}}\left(S^b_{\mathrm{i}} S^b_{\mathrm{j}} - S^a_{\mathrm{i}} S^a_{\mathrm{j}}\right). \end{aligned} \tag{3}$$

Two distinct antiferromagnetic (AFM) interlayer stacking patterns are found in the K_2NiF_4-type oxides depending on j_c and δ_c. For example, tetragonal La_2NiO_4 and Sr_2IrO_4 crystals show the AFM-1 type [9–13], whereas orthorhombic La_2CuO_4 crystals exhibit the AFM-2 type [14–17], as shown in Fig. 1(b). La_2CoO_4 crystals present both types depending upon their phase transitions between tetragonal and orthorhombic structures [18]. On the other hand, by applying external stimuli such as pressure, the frustrated interlayer interaction leads to the suppression of the interlayer magnetic order, enhancing the quantum fluctuation that can open a path to quantum paramagnetic phases [19].

In the tetragonal structure, the AFM stacking order is correlated with anisotropic interlayer pseudodipolar interaction since the interlayer exchange interaction cancels out, i.e., AFM-1 for $\delta_c < 0$ and AFM-2 for $\delta_c > 0$ [12]. On the other hand, the interlayer exchange interaction is also an important factor to determine the stacking order in the orthorhombic structure. Therefore, one may conjecture that AFM-2 type order can be induced when orthorhombic distortion is applied to a tetragonal system. However, recent experiments by Kim *et al.* showed that the AFM-1 type order remained in the

---

[*] a.seo@uky.edu

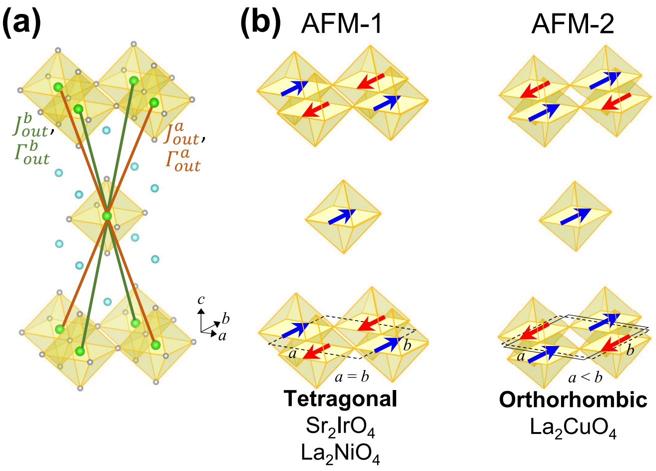

FIG. 1. (a) A schematic crystal structure of K_2NiF_4-type oxides. The interlayer exchange interactions J^a_{out} and J^b_{out} share the same interaction paths with the interlayer pseudodipolar interactions Γ^a_{out} and Γ^b_{out}, respectively. (b) Schematic diagrams of two different long-range antiferromagnetic (AFM) stacking patterns in the K_2NiF_4-type oxides. The AFM-1 type is observed in tetragonal Sr_2IrO_4 and La_2NiO_4 crystals, whereas the AFM-2 type is observed in orthorhombic La_2CuO_4 crystals.

Sr_2IrO_4 crystals even under orthorhombic distortion using a piezoelectric strain device [20]. Hence, the interlayer AFM stacking order would be irrelevant to the crystal structure, or the magnitude of the orthorhombic distortion (~0.03%) was not large enough to stabilize the AFM-2 type stacking pattern in the Sr_2IrO_4 crystals. It is formidable to figure out which one is correct because conventional strain/stress device approaches using bulk crystals cannot exert much larger external pressure than the magnitude used in the studies of Ref. [20].

In this Letter, we report that the long-range AFM-2 stacking order emerges in the layered iridate Sr_2IrO_4 thin films when substantially large (>1.5%) orthorhombic distortion is applied via biaxial strain. Such a large magnitude of orthorhombic distortion is realized by constructing epitaxial thin-film heterostructures of $Sr_2IrO_4/Ca_3Ru_2O_7$ with excellent structural coherence and atomically sharp interfaces. We observed clear magnetic Bragg reflections from the Ir L_3-edge resonant x-ray scattering experiments, indicating that the AFM-2 type stacking order is stabilized when $|j_c|$ exceeds $|\delta_c|$. Our result confirms that the long-range AFM stacking order of the quasi-two-dimensional oxides is correlated with their crystal structures. It is noteworthy that our experimental finding provides a useful approach for enhancing the magnetic frustrations (i.e., magnetic quantum fluctuations) of various two-dimensional magnetic systems via utilizing the subtle competition between the interlayer exchange interaction and the pseudodipolar interaction.

We conceived $Sr_2IrO_4/Ca_3Ru_2O_7$ heterostructures to study the effect of orthorhombic distortion to the AFM order because of the large anisotropic lattice mismatch between the tetragonal Sr_2IrO_4 and the orthorhombic $Ca_3Ru_2O_7$, i.e., −2.22% and +0.45% along the *a* and *b* directions, respectively, as shown in Fig. 2(a). The heterostructure samples were synthesized by depositing 24-nm-thick Sr_2IrO_4 epitaxial thin films on $Ca_3Ru_2O_7$ single crystals with cleaved (0 0 1)-surfaces using pulsed laser deposition (PLD). The PLD

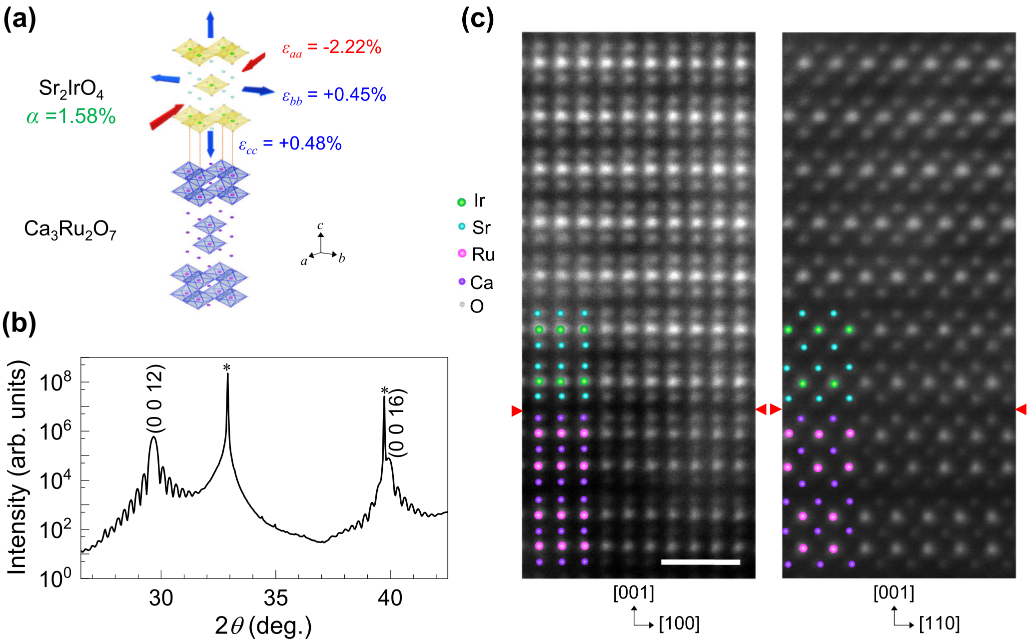

FIG. 2. (a) A schematic diagram of a $Sr_2IrO_4/Ca_3Ru_2O_7$ heterostructure. The red and blue arrows represent compressive and tensile strain directions and magnitudes. (b) X-ray diffraction (0 0 L) scan of a $Sr_2IrO_4/Ca_3Ru_2O_7$ heterostructure. The (0 0 12) and (0 0 18) peaks from the Sr_2IrO_4 thin film are visible. The asterisks [*] indicate the peaks from the $Ca_3Ru_2O_7$ single-crystal substrate. (c) High-resolution Z-contrast STEM images of a $Sr_2IrO_4/Ca_3Ru_2O_7$ heterostructure for two different cross-sectional directions. The red triangles mark the atomically sharp interface between Sr_2IrO_4 and $Ca_3Ru_2O_7$. The scale bar is 1 nm.

TABLE I. Lattice constants and strain values of Sr_2IrO_4 (001) epitaxial thin films grown on $Ca_3Ru_2O_7$ (001) single crystals.

	a (Å)	b (Å)	c (Å)	α (%)[a]	ε_{aa} (%)	ε_{bb}(%)	ε_{cc}(%)	V(Å^3)
$Ca_3Ru_2O_7$ substrate 8 K [27]	5.367	5.536	19.521					
$Ca_3Ru_2O_7$ substrate 296 K [27]	5.378	5.523	19.587					
Sr_2IrO_4 thin films 6 K	5.364(4)	5.536(4)	25.92(2)	+1.58	−2.21(7)	+0.93(7)	+0.47(8)	769.9
Sr_2IrO_4 thin films 296 K	5.378(4)	5.523(4)	25.94(2)	+1.33	−2.22(9)	+0.44(8)	+0.61(8)	770.5

[a] Values are obtained using $\alpha \equiv (b-a)/(b+a) \times 100(\%)$.

conditions are a laser fluence of 1.2 J/cm^2, a substrate temperature of 700 °C, and an oxygen partial pressure of 10 mTorr, values which are consistent with Ref. [21]. Figure 2(b) shows x-ray diffraction with well-defined (0 0 L) peaks and Kiessig fringes from a $Sr_2IrO_4/Ca_3Ru_2O_7$ heterostructure, indicating a high-quality thin film with a thickness of ∼24 nm. The structural coherence length of ∼29 nm, obtained from the FWHM of the (0 0 20) peak, is comparable to the thickness of the Sr_2IrO_4 thin film (Fig. S1(c) [22]). The H and K scans near (2 0 20) and (0 2 20) reflections, respectively, show that the Sr_2IrO_4 thin films are fully strained along both in-plane directions (Figs. S1(a) and (b) [22]). Large in-plane anisotropy with −2.21% compressive strain along the a axis and +0.93% tensile strain along the b axis is observed in these thin films (Table I), which correspond to the significantly large orthorhombic distortion [$\alpha \equiv (b-a)/(b+a)$] of +1.58% at low temperature (6 K). Considering Young's modulus of ∼130 GPa of Sr_2IrO_4 crystals [23], this compressive strain corresponds to an effective uniaxial pressure of ∼2.9 GPa along the a axis, which is far above the accessible range of conventional strain/stress approaches [24]. This anisotropic strain is expected to lower the crystal symmetry of Sr_2IrO_4 from tetragonal to orthorhombic, as shown in Fig. 2(a). Structural Bragg peaks of (1 2 19) and (1 2 21) that are relevant to the octahedral rotation along the c axis [25,26] were not observed from our samples (Fig. S1(d) [22]), implying that the octahedral rotational pattern is substantially modified in these $Sr_2IrO_4/Ca_3Ru_2O_7$ heterostructures, presumably due to the large orthorhombic distortion. Figure 2(c) shows high-resolution Z-contrast scanning transmission electron microscopy (STEM) data of the cross sections of the heterostructures. Note that an atomically sharp interface between Sr_2IrO_4 and $Ca_3Ru_2O_7$ is observed without any noticeable misfit dislocations or atomic intermixing even under such a large orthorhombic distortion.

Resonant x-ray scattering experiments reveal an unprecedented AFM-2 stacking order which has not been observed from any Sr_2IrO_4 crystals or thin films. Using resonant x-ray near the Ir L_3 edge ($\hbar\omega = 11.217$ keV as shown in Fig. S3(f) [22]), we observed a clear (1 0 24) magnetic Bragg peak at 6 K with a magnetic coherence length of ∼26 nm along the out-of-plane direction (Fig. S3(b) [22]), comparable to the out-of-plane structural coherence length of ∼29 nm (Fig. S1(c) [22]). Figure 3(a) shows the azimuthal angle (Ψ) dependence of the (1 0 24) magnetic Bragg peak (see Fig. S4(a) [22]) in which the sample is rotated about the scattering vector with $\Psi = 0$ defined such that the crystallographic a axis lies in the scattering plane as shown in Fig. S3(e) [22]. We used the σ - π polarization channel of the incoming and outgoing x-rays because the magnetic Bragg peak intensities follow the relation $I \propto |\vec{m} \cdot (\sigma_i \times \sigma_o')|^2$, where σ_i and σ_o' are the incoming and outgoing polarizations of photons and $\vec{m}$ is the $J_{\rm eff} = 1/2$ pseudospin magnetic moment [28,29]. We observed that the azimuthal angle dependence of the integrated peak intensity, obtained by fitting the Gaussian peak shape of L scans, follows the theoretical calculation for $\vec{m} \parallel \vec{b}$. This observation indicates that the magnetic moment is along the crystallographic b axis without any secondary magnetic domains of $\vec{m} \parallel \vec{a}$. Note that this observation of $\vec{m} \parallel \vec{b}$ is consistent with the result of Ref. [20] in which the orthorhombic distortion of ∼0.03% is applied using uniaxial compressive strain along the a axis of a Sr_2IrO_4 single crystal. These two results confirm that the uniaxial magnetic anisotropy due to orthorhombic distortion is crucial in determining the direction of the magnetic moment with respect to the crystallographic axis [30].

Figure 3(b) shows that the integrated intensity of the magnetic Bragg peak (see Fig. S4(b) [22]) decreases with increasing temperature, suggesting the long-range AFM order below $T_N = 222$ K. Note that this value of T_N is comparable to that of Sr_2IrO_4 single crystals (<230 K) [31–33] despite the orthorhombic distortion. The integrated intensity follows the power-law scaling function $I(t) \approx |t|^{2\beta}$ with the critical exponent $\beta = 0.22$, where $t \equiv 1-\frac{T}{T_N}$ is the reduced temperature, as shown in the inset of Fig. 3(b). The critical exponent (0.22), corresponding to the 2D XYh_4 universality class similar to the bulk crystal, seems reasonable for this quasi-2D system with weak interlayer coupling [34–36].

Full (0 1 L) and (1 0 L) scans over the wide range of L from 15 to 25 reciprocal lattice units show clear (1 0 4n) and (0 1 4n+2) magnetic Bragg peaks with n = 4, 5, and 6, as shown in Fig. 4(a). Additional strong structural Bragg reflections from the $Ca_3Ru_2O_7$ crystal are indicated by asterisks (*). Note that these magnetic Bragg peaks, i.e., (1 0 4n) and (0 1 4n+2) with $\vec{m} \parallel \vec{b}$, are the ones expected in the AFM-2 type stacking order [12] which is observed in orthorhombic systems such as La_2CuO_4 [14–16]. In tetragonal Sr_2IrO_4 crystals, the AFM-2 type stacking order is energetically $2|\delta_c|$ higher than the AFM-1 type stacking order, which allows (1 0 4n+2) and (0 1 4n) with $\vec{m} \parallel \vec{b}$ [12].

Our experimental finding not only confirms that the interlayer AFM order is correlated with crystal symmetry but also leads us to further understand the competition between j_c and δ_c in determining the long-range AFM order in the system, as schematically shown in Fig. 4(b):

(1) Where the orthorhombic distortion (α) is zero, tetragonal Sr_2IrO_4 crystals have isotropic $J_{\rm out}$, i.e., $J^a_{\rm out} = J^b_{\rm out}$, resulting in $j_c = 0$ for the G-type AFM order. Two equivalent AFM domains with the AFM-1 type stacking order with $\vec{m} \parallel \vec{a}$ and $\vec{m} \parallel \vec{b}$ are stabilized with the energy of $\delta_c < 0$. They correspond to *uudd* and *lrrl* stacking order discussed in Ref. [12].

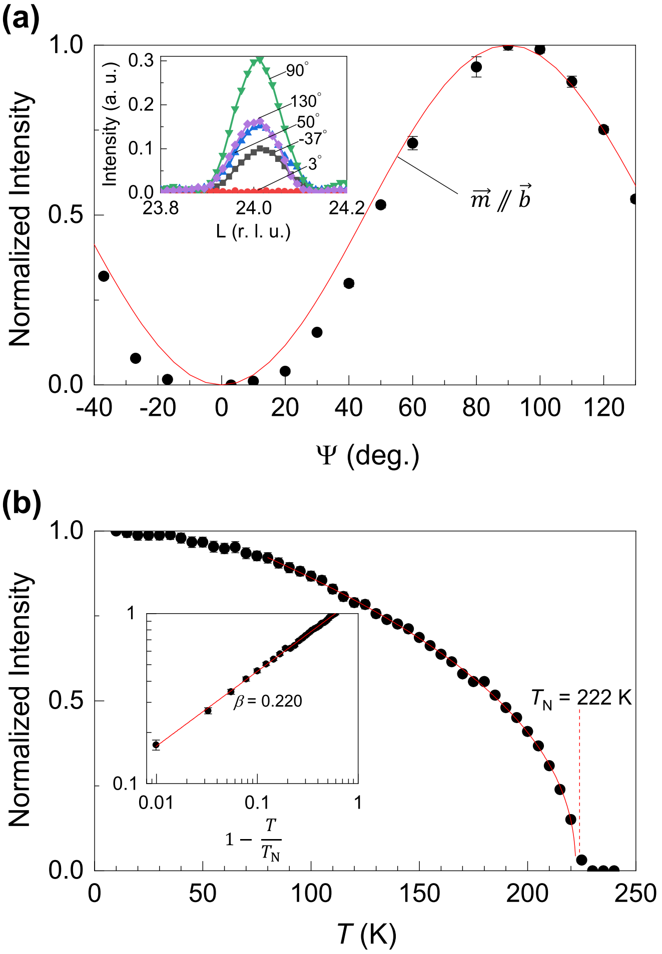

FIG. 3. (a) Normalized integrated intensities of the Ir L_3-edge (1 0 24) magnetic Bragg peaks of a $Sr_2IrO_4/Ca_3Ru_2O_7$ heterostructure as a function of azimuthal angle (Ψ) with σ - π polarization channel. The solid (red) line represents a theoretical calculation for the $J_{\rm eff} = {}^1/_2$ pseudospin magnetic moment ($\vec{m}$) parallel to the crystallographic b axis, as shown in the schematic diagram. $\Psi = 0$ is defined as the crystallographic a axis lying in the scattering plane. The inset shows the same magnetic Bragg peak intensities at selected azimuthal angles. (b) Normalized integrated intensities of the (1 0 24) magnetic Bragg peaks as a function of temperature. The solid (red) line is a power-law fit using the equation $I \propto [1-\frac{T}{T_N}]^{2\beta}$, where T_N and β are the Néel temperature (~222 K) and the critical exponent, respectively. (Inset) Normalized integrated intensity vs the reduced temperature $(1-\frac{T}{T_N})$ in the logarithmic scale. The estimated critical exponent $\beta = 0.22$ is close to 0.23 corresponding to the 2D XYh_4 universality model [33,34].

(2) $0 < \alpha < \alpha_c$, where α_c is a critical value, as the tetragonal structure of Sr_2IrO_4 becomes an orthorhombic structure, the AFM-1 type order with $\vec{m} \parallel \vec{b}$ is stabilized over the other phase with $\vec{m} \parallel \vec{a}$ due to the pseudospin-lattice interaction within the IrO_2 basal planes. This transition was experimentally observed with $\alpha \approx 0.03\%$ [20]. $J_{\rm out}$ is no longer isotropic, i.e., $J^a_{\rm out} > J^b_{\rm out}$, resulting in nonzero j_c. Nevertheless, the interlayer pseudodipolar interaction remains dominant since $|j_c| < |\delta_c|$.

(3) $\alpha > \alpha_c$, the interlayer exchange interaction becomes dominant over the pseudo-dipolar interaction, i.e., $j_c + \delta_c < 0$ with $|j_c| > |\delta_c|$, making the AFM-2 type stacking order stabilized. Using the tight-binding approximation, we can estimate the value of j_c to be around -0.9 μeV ($\alpha = 1.6\%$), whose magnitude is larger than the estimated value of $\delta_c = 0.3$ μeV.

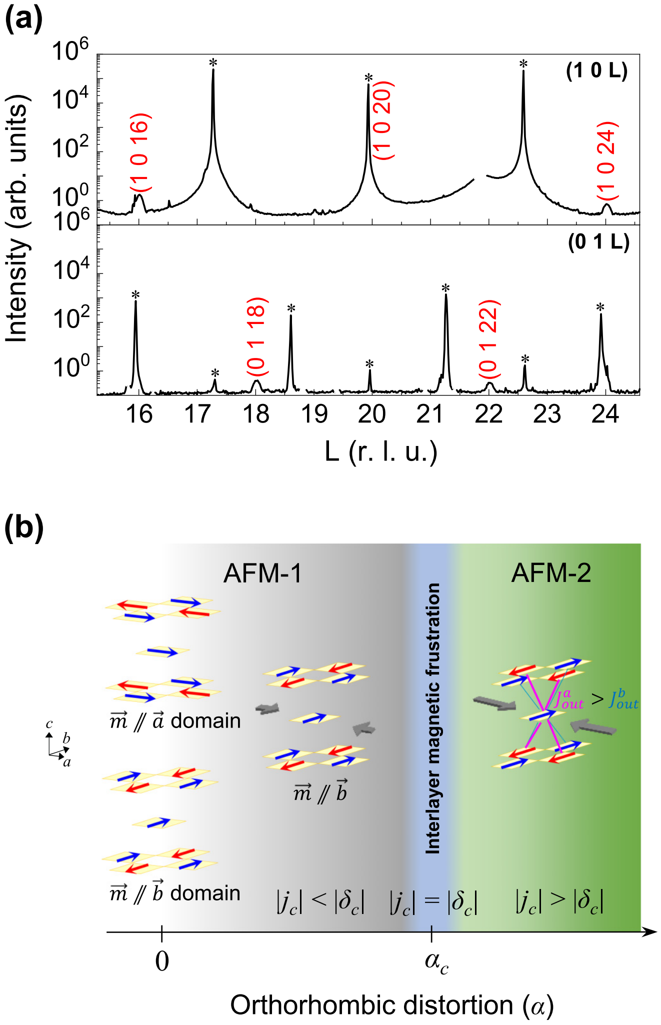

FIG. 4. (a) Ir L_3-edge x-ray (1 0 L) and (0 1 L) scans of a $Sr_2IrO_4/Ca_3Ru_2O_7$ heterostructure at 6 K. (1 0 16), (1 0 20), (1 0 24), (0 1 18), and (0 1 22) magnetic Bragg peaks are observed. The asterisks [*] indicate the peaks from the $Ca_3Ru_2O_7$ single-crystal substrate. (b) A schematic phase diagram of AFM stacking orders of Sr_2IrO_4 as a function of orthorhombic distortion. When $\alpha = 0$, i.e., a tetragonal structure, equivalent twin domains (AFM-1) can coexist. With increasing the orthorhombic distortion (α) up to the critical point (α_c), the magnetic domains are just detwinned. With larger orthorhombic distortion than α_c, the AFM-2 type stacking order is stabilized, exhibiting the magnetic moment parallel to the b axis and the magnetic Bragg peaks of (1 0 4n) and (0 1 4n+2).

(4) $\alpha \approx \alpha_c$, both AFM-1 and AFM-2 type stacking orders can coexist due to $|j_c| \approx |\delta_c|$, meaning that the system has a large interlayer magnetic frustration and consequently enhances the magnetic quantum fluctuation. By assuming $\delta_c = 0.3$ μeV (Ref. [12]) and linear extrapolation between our experimental values, α_c is estimated to be around +0.7%. It would be a formidable task to experimentally study the interlayer magnetic frustration near the critical value. However, applying a gradual strain to obtain continuous orthorhombic

distortion in freestanding nanomembranes [37] could provide an accessible approach.

Our result suggests that the competition between interlayer exchange interaction and pseudodipolar interaction provides an intriguing tuning parameter to stabilize the long-range magnetic stacking order in quasi-2D systems. We have observed a distinct La_2CuO_4-like AFM stacking order in Sr_2IrO_4 by enhancing $|j_c|$ over $|\delta_c|$ via large orthorhombic distortion. In addition to opening exciting questions on the detailed nature of the competition between interlayer interactions, these results raise the prospects of tuning the anisotropic coupling between spins into exotic quantum phases.

We acknowledge the support of National Science Foundation Grants No. DMR-1454200, No. DMR-2011876, and No. DMR-2104296 for sample synthesis and characterization. This research used resources of the Advanced Photon Source, a U.S. Department of Energy (DOE) Office of Science User Facility, operated for the DOE Office of Science by Argonne National Laboratory under Contract No. DE-AC02-06CH11357. Electron microscopy was performed at the Center for Electron Microscopy and Analysis at the Ohio State University. B.K. acknowledges financial support from the Deutsche Forschungsgemeinschaft (DFG, German Research Foundation) through Project No. 107745057-TRR 80.

---

[1] P. M. Grant, S. S. P. Parkin, V. Y. Lee, E. M. Engler, M. L. Ramirez, J. E. Vazquez, G. Lim, R. D. Jacowitz, and R. L. Greene, Phys. Rev. Lett. **58**, 2482 (1987).

[2] J. Orenstein and A. J. Millis, Science **288**, 468 (2000).

[3] M. Imada, A. Fujimori, and Y. Tokura, Rev. Mod. Phys. **70**, 1039 (1998).

[4] B. J. Kim, H. Ohsumi, T. Komesu, S. Sakai, T. Morita, H. Takagi, and T. Arima, Science **323**, 1329 (2009).

[5] B. J. Kim, H. Jin, S. J. Moon, J.-Y. Kim, B.-G. Park, C. S. Leem, J. Yu, T. W. Noh, C. Kim, S.-J. Oh, J.-H. Park, V. Durairaj, G. Cao, and E. Rotenberg, Phys. Rev. Lett. **101**, 076402 (2008).

[6] V. M. Katukuri, V. Yushankhai, L. Siurakshina, J. van den Brink, L. Hozoi, and I. Rousochatzakis, Phys. Rev. X **4**, 021051 (2014).

[7] P. A. Lee, N. Nagaosa, and X.-G. Wen, Rev. Mod. Phys. **78**, 17 (2006).

[8] N. D. Mermin and H. Wagner, Phys. Rev. Lett. **17**, 1133 (1966).

[9] J. Rodriguez-Carvajal, M. T. Fernandez-Diaz, and J. L. Martinez, J. Phys.: Condens. Matter **3**, 3215 (1991).

[10] T. M. Brill, G. Hampel, F. Mertens, R. Schurmann, W. Assmus, and B. Luthi, Phys. Rev. B **43**, 10548 (1991).

[11] C. Dhital, T. Hogan, Z. Yamani, C. de la Cruz, X. Chen, S. Khadka, Z. Ren, and S. D. Wilson, Phys. Rev. B **87**, 144405 (2013).

[12] J. Porras, J. Bertinshaw, H. Liu, G. Khaliullin, N. H. Sung, J.-W. Kim, S. Francoual, P. Steffens, G. Deng, M. M. Sala, A. Efimenko, A. Said, D. Casa, X. Huang, T. Gog, J. Kim, B. Keimer, and B. J. Kim, Phys. Rev. B **99**, 085125 (2019).

[13] F. Ye, S. Chi, B. C. Chakoumakos, J. A. Fernandez-Baca, T. Qi, and G. Cao, Phys. Rev. B **87**, 140406(R) (2013).

[14] D. Vaknin, S. K. Sinha, D. E. Moncton, D. C. Johnston, J. M. Newsam, C. R. Safinya, and H. E. King Jr., Phys. Rev. Lett. **58**, 2802 (1987).

[15] T. Freltoft, J. P. Remeika, D. E. Moncton, A. S. Cooper, J. E. Fischer, D. Harshman, G. Shirane, S. K. Sinha, and D. Vaknin, Phys. Rev. B **36**, 826(R) (1987).

[16] M. Reehuis, C. Ulrich, K. Prokeš, A. Gozar, G. Blumberg, S. Komiya, Y. Ando, P. Pattison, and B. Keimer, Phys. Rev. B **73**, 144513 (2006).

[17] Y. S. Lee, R. J. Birgeneau, M. A. Kastner, Y. Endoh, S. Wakimoto, K. Yamada, R. W. Erwin, S. H. Lee, and G. Shirane, Phys. Rev. B **60**, 3643 (1999).

[18] K. Yamada, M. Matsuda, Y. Endoh, B. Keimer, R. J. Birgeneau, S. Onodera, J. Mizusaki, T. Matsuura, and G. Shirane, Phys. Rev. B **39**, 2336 (1989).

[19] D. Haskel, G. Fabbris, J. H. Kim, L. S. I. Veiga, J. R. L. Mardegan, C. A. Escanhoela, Jr., S. Chikara, V. Struzhkin, T. Senthil, B. J. Kim *et al.*, Phys. Rev. Lett. **124**, 067201 (2020).

[20] J.-W. Kim, S. H. Chun, Y. Choi, B. J. Kim, M. H. Upton, and P. J. Ryan, Phys. Rev. B **102**, 054420 (2020).

[21] S. S. A. Seo, J. Nichols, J. Hwang, J. Terzic, J. H. Gruenewald, M. Souri, J. Thompson, J. G. Connell, and G. Cao, Appl. Phys. Lett. **109**, 201901 (2016).

[22] See Supplemental Material at http://link.aps.org/supplemental/10.1103/PhysRevB.105.L100404 for more details on the structural information and the resonant x-ray scattering experiments.

[23] A. Jain, S. P. Ong, G. Hautier, W. Chen, W. D. Richards, S. Dacek, S. Cholia, D. Gunter, D. Skinner, G. Ceder *et al.*, APL Mater. **1**, 011002 (2013).

[24] J. Park, J. M. Bartlett, H. M. L. Noad, A. L. Stern, M. E. Barber, M. Konig, S. Hosoi, T. Shibauchi, A. P. Mackenzie, A. Steppke *et al.*, Rev. Sci. Instrum. **91**, 083902 (2020).

[25] M. K. Crawford, M. A. Subramanian, R. L. Harlow, J. A. Fernandez-Baca, Z. R. Wang, and D. C. Johnston, Phys. Rev. B **49**, 9198 (1994).

[26] S. Geprägs, B. E. Skovdal, M. Scheufele, M. Opel, D. Wermeille, P. Thompson, A. Bombardi, V. Simonet, S. Grenier, P. Lejay *et al.*, Phys. Rev. B **102**, 214402 (2020).

[27] Y. Yoshida, S.-I. Ikeda, H. Matsuhata, N. Shirakawa, C. H. Lee, and S. Katano, Phys. Rev. B **72**, 054412 (2005).

[28] J. P. Hill and D. F. McMorrow, Acta Cryst. A **52**, 236 (1996).

[29] M. Moretti Sala, S. Boseggia, D. F. McMorrow, and G. Monaco, Phys. Rev. Lett. **112**, 026403 (2014).

[30] H. Zhang, L. Hao, J. Yang, J. Mutch, Z. Liu, Q. Huang, K. Noordhoek, A. F. May, J. H. Chu, J. W. Kim *et al.*, Adv. Mater. **32**, 2002451 (2020).

[31] H. Wang, C. Lu, J. Chen, Y. Liu, S. L. Yuan, S. W. Cheong, S. Dong, and J. M. Liu, Nat. Commun. **10**, 2280 (2019).

[32] M. Ge, T. F. Qi, O. B. Korneta, D. E. De Long, P. Schlottmann, W. P. Crummett, and G. Cao, Phys. Rev. B **84**, 100402(R) (2011).

[33] G. Cao, J. Bolivar, S. McCall, J. E. Crow, and R. P. Guertin, Phys. Rev. B **57**, R11039 (1998).

[34] A. Taroni, S. T. Bramwell, and P. C. Holdsworth, J. Phys.: Condens. Matter **20**, 275233 (2008).

[35] S. T. Bramwell and P. C. W. Holdsworth, J. Phys.: Condens. Matter **5**, 53 (1993).

[36] J. G. Vale, S. Boseggia, H. C. Walker, R. Springell, Z. Feng, E. C. Hunter, R. S. Perry, D. Prabhakaran, A. T. Boothroyd, S. P. Collins *et al.*, Phys. Rev. B **92**, 020406(R) (2015).

[37] S. Shrestha, M. Coile, M. Zhu, M. Souri, J. Kim, R. Pandey, J. W. Brill, J. Hwang, J.-W. Kim, and A. Seo, ACS Appl. Nano Mater. **3**, 6310 (2020).